

Fig. 2. Activation variable  $m$ . **a**, Dynamics of  $m$  as measured through  $I_T$ , in response to step changes of the membrane voltage  $V_M$  (shown at bottom).  $V_M$  begins low so that  $m = 0$ , and steps to higher voltages. **b**, Voltage-dependence of  $m$ 's steady-state, as measured through  $I_T$  by sweeping  $V_M$  slowly (normalized). The fit is to Eqn. 3. **c**, Voltage-dependence of  $m$ 's time-constant, extracted by fitting the measurements in **a** to the solution of Eqn. 1 for step changes in  $V$ . The fit is to Eqn. 4.

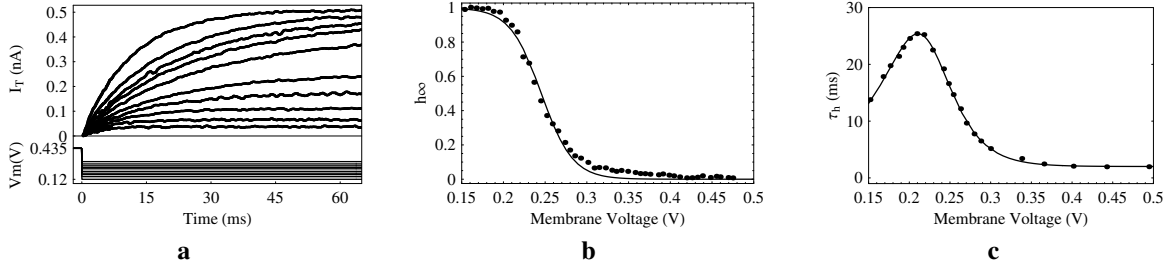


Fig. 3. Inactivation variable  $h$ . **a**, Dynamics of  $h$  as measured through  $I_T$ , in response to step changes of the membrane voltage  $V_M$  (shown at bottom). **b**, Voltage-dependence of  $h$ 's steady-state, as measured through  $I_T$  by sweeping  $V_M$  slowly (normalized). The fit is to Eqn. 3. **c**, Voltage-dependence of  $h$ 's time-constant. We extracted the time-constant from **a**, obtained as in Fig. 2c. The fit is to Eqn. 4.

$$\begin{aligned} I_T &= I_{ds0} e^{\kappa m_V - m_C} e^{(1-\kappa)(h_V - h_{b1k})} \\ &= m^\kappa h \bar{I}_T, \end{aligned} \quad (2)$$

where  $m = e^{m_V - m_H}$ ,  $h = e^{(1-\kappa)(h_V - h_{b1k})}$ , and  $\bar{I}_T = I_{ds0} e^{\kappa m_H - m_C}$  (the maximum T-channel current). Note that all voltages here, and in further equations, are in units of the thermal voltage  $U_T$ . We describe the activation and inactivation subcircuits next.

#### A. Activation Variable $m$

For our activation subcircuit, we use a previously published design [2], which requires only three transistors to achieve the steady-state's and time-constant's voltage-dependencies. N11's current represents the activation rate, which increases when  $V_M$ —the dendritic membrane voltage—increases. N9's current represents the deactivation rate, which increases with  $V_N$ —the inverted dendritic membrane voltage, produced by a negative-gain amplifier. Thus, when  $V_M$  increases,  $V_N$  decreases, and  $m_V$  moves towards  $m_H$ , increasing  $m$ . When  $V_M$  decreases,  $V_N$  increases, and  $m_V$  moves toward  $m_L$ , decreasing  $m$ . The time-constant is inversely related to the sum of the rates; we use  $m_{PK}$  to limit the magnitude of the N11's current, fixing the minimum time-constant at large membrane voltages.

The steady-state's and time-constant's voltage-dependencies, derived using the subthreshold MOS transistor equations [2], are:

$$m_\infty(V_M) = \frac{1}{1 + \exp\left[-\frac{V_M - V_m^{\text{mid}}}{V_m^*}\right]} \quad (3)$$

$$\frac{\tau_m(V_M)}{\hat{\tau}_m} = 1 + \frac{1}{\exp\left(\frac{V_M - V_{1m}}{\sqrt{V_{1m}^*}}\right) + \exp\left(-\frac{V_M - V_{2m}}{\sqrt{V_{2m}^*}}\right)} \quad (4)$$

where  $\hat{\tau}_m = (C_M U_T / I_{ds0}) e^{m_H - \kappa m_{PK}}$  is the time-constant at high and low membrane voltages;  $V_m^{\text{mid}}$ ,  $V_{1m}$ ,  $V_{2m}$  are functions of the voltage biases  $m_H$ ,  $m_L$ ,  $m_{PK}$  and  $n_{VN}$  (see Fig. 4); and  $V_m^*$ ,  $V_{1m}^*$ ,  $V_{2m}^*$  are determined by the transistor parameters  $\kappa$  and  $U_T$  (see [2] for more details).

Since  $I_T = m^\kappa h \bar{I}_T$ , we can record the dynamics of  $m$  by fixing the inactivation variable  $h$  and measuring  $I_T$ , stepping  $V_M$  to increasingly higher voltages (Fig. 2a). We notice two effects: The steady-state increases with the step-size, and the rate at which the output reaches steady-state changes, slowing down initially, but then speeding back up again. We extract the time-constant's voltage-dependence from these curves, and measure the steady-state's voltage-dependence by sweeping  $V_M$  slowly and recording  $I_T$ . Our experimental results are in good agreement with Eqns. 3 and 4 (Fig. 2b and Fig. 2c).

#### B. Inactivation Variable $h$

The inactivation subcircuit's operation is similar in principle to the activation subcircuit's. Whereas the activation subcircuit operates by modulating N10's source ( $m_V$ ) to match its current with N9's, the activation subcircuit operates by modulating P4's well ( $h_V$ ) to match the currents in P2 and P5. We use the PMOS's back-gate to achieve longer time-constants, as the back-gate's voltage has to change more than the gate's due to the former's weaker influence on current. This is equivalent to increasing the capacitor  $C_h$ , but is more efficient in surface area.

The differential equation describing  $h_V$  is:

$$C_h \frac{dh_V}{dt} = I_2 + I_1 - I_1 e^{-(1-\kappa)(h_V - h_{b1k})},$$

where the gain on the last term comes from the mirror P3-4. Recall that  $h = e^{(1-\kappa)(h_V - h_{b1k})}$ , therefore

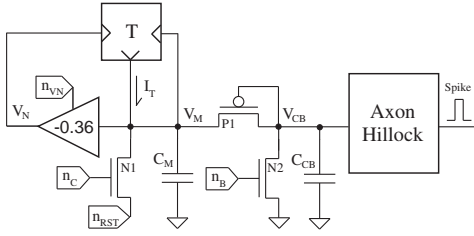


Fig. 4. Our neuron circuit is a two-compartment model of the relay cell:  $C_M$  represents the dendrite, and  $C_{CB}$  represents the cell body. The T-channel (T) is described in Fig. 1. The Axon Hillock generates a spike once  $V_{CB}$  reaches a fixed threshold, and then resets  $V_{CB}$  to Gnd. The amplifier inverts  $V_M$  with a gain of  $-0.36$ ;  $V_N = n_{VN}$ , an adjustable bias, when  $V_M = 0$  (Gnd).

$$\begin{aligned} Q_h \frac{1}{h} \frac{dh}{dt} &= - \left( \frac{1}{h} - 1 \right) I_1 + I_2 \\ \frac{dh}{dt} &= - \frac{I_1 + I_2}{Q_h} \left( h - \frac{I_1}{I_1 + I_2} \right) \end{aligned} \quad (5)$$

where  $Q_h = C_h U_T / (1 - \kappa)$ . Eqn. 5 is now equivalent to Eqn. 1, as both  $I_1$  and  $I_2$  are functions of  $V_M$ . Through algebraic manipulation of transistor equations [3], we can show the  $h$ 's steady-state and time-constant have the same form as Eqns. 3 and 4, except  $\hat{\tau}_h = (C_h U_T / I_{ds0}) e^{h_{TG} - \kappa h_T} / (1 - \kappa)$ ; and  $V_h^{\text{mid}}$ ,  $V_{1h}$ ,  $V_{2h}$  are determined by  $h_T$  and  $n_{VN}$ ;  $V_h^*$ ,  $V_{1h}^*$ , and  $V_{2h}^*$  are determined by  $\kappa$  and  $U_T$ . The factor  $(1 - \kappa)$  in  $\hat{\tau}_h$  derives from the use of the back-gate.

Like the activation variable, we can record the dynamics of  $h$  through  $I_T$  by fixing  $m$  (Fig. 3a). Stepping  $V_M$  to increasingly lower voltages, we notice an increase in the steady-state and a non-monotonic change in time-constant. These measured voltage-dependencies agree well with Eqns. 3 and 4 (Fig. 3b and Fig. 3c).

### III. SILICON RELAY CELL

In this section, we attach our T-channel circuit to a silicon neuron, and use injected currents to probe the channel's influence on the cell's response. After describing the relay neuron circuit, we demonstrate the two response modes—tonic and burst—with input current steps. However, the T-channel can produce a graded response between these two extremes.  $I_T$ 's current amplitude depends on the degree of priming—the duration and magnitude of pre-burst inhibition. We demonstrate this using sinusoidal input currents of varying frequency and mean level.

We fabricated 7200 relay neurons on a  $11.5\text{mm}^2$  chip in  $0.25\mu\text{m}$  CMOS, each neuron approximately  $774\mu\text{m}^2$  in area. Surrounding the neural core is digital circuitry that controls action potential communication into, and out of, the network. The chip possesses a total of 110 I/O pads.

#### A. Cell Circuit

We use a two-compartment model for our cell (Fig. 4): One compartment represents the dendrite, the other, the cell body. The dendritic compartment has a membrane capacitor ( $C_M$ ) and a leak (N1). The T-channel's current  $I_T$  drives  $V_M$ . Absent any input, the leak causes  $V_M$  to rest at  $n_{RST}$ . When the net input current is negative,  $V_M$  drops until N1's current matches the input. When the net input current is positive,  $V_M$  rises until P1 turns on and passes current into the cell body compartment.

The cell body compartment has three components: a membrane capacitor ( $C_{CB}$ ), a leak transistor (N2), and an axon-hillock circuit.

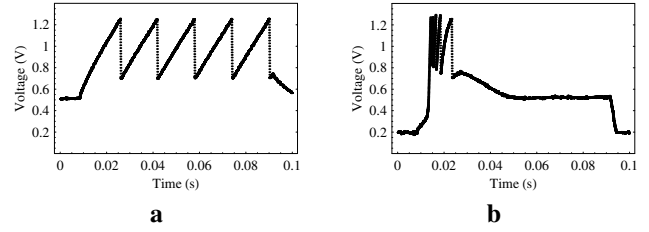


Fig. 5. Dendritic voltage ( $V_M$ ) records of the relay cell's two response modes: **a** Tonic; **b** Burst. In tonic-mode,  $V_M$  is initially high ( $\approx 500\text{mV}$ ), which inactivates  $I_T$ . In burst-mode,  $V_M$  is initially low ( $\approx 200\text{mV}$ ), which deinactivates  $I_T$ . An 80ms-wide current step is injected into the dendritic compartment at 10ms in both cases.

Current from the dendritic compartment integrates on  $C_{CB}$ . Once  $V_{CB}$  surpasses a voltage threshold, the axon hillock circuit—a modified version of the one in [4]—generates a spike. A reset transistor within the Axon Hillock then turns on, pulling  $V_{CB}$  down to Gnd, and then the cell starts to integrate current from the dendritic compartment again. We connect the source of the leak transistor to Gnd rather than a voltage bias (such as  $n_{RST}$  in the dendrites) because there are no inhibitory dynamics within the cell body, allowing us to use the whole voltage range from Gnd to threshold during input integration. The reset current within the cell body also affects  $V_M$  through P1. However, rather than reset to Gnd,  $V_M$  only resets partially due to the voltage-drop across P1 (see Fig. 5a).

#### B. Step Current Response

We first show the cell's response to a step current in the dendritic compartment (Fig. 5a). With no input,  $V_M \approx 500\text{mV}$ , sufficiently high to inactivate the T-channel. After the step,  $V_M$  begins to rise, and current eventually passes into the somatic compartment ( $C_{CB}$ ).  $V_M$  increases linearly until  $V_{CB}$  reaches spike threshold, and an output spike is generated (not shown).  $V_{CB}$  resets to Gnd, and  $V_M$ , through the action of transistor P1, resets to approximately  $700\text{mV}$ . After reset, dendritic integration continues. Since  $V_M$ 's trajectory is linear, the firing rate increases linearly with input current (data not shown), as observed in real relay cells [5].

Next, we repeat the procedure with a constant inhibitory current added to the injected current step (Fig. 5b). The inhibitory current lowers  $V_M$  to approximately  $200\text{mV}$ , thereby deinactivating  $I_T$  (i.e.,  $h$  increases). After the step,  $V_M$  begins to rise; at around  $400\text{mV}$ ,  $I_T$  turns on, causing a rapid rise in  $V_M$  and initiating a burst. The initial spike rate approaches  $1\text{kHz}$ , decreasing with each successive spike as  $h$  decreases, and eventually the cell stops firing.

Since the cell stops spiking once T-channel inactivates, we know that the cell would not spike absent  $I_T$ . This demonstrates that without the channel (i.e., in tonic-mode), the cell's response is completely dependent on the input, firing spikes at a rate that is a function of the input. With the channel, (i.e., in burst-mode), the cell's response no longer reflects the magnitude of the input; rather, the cell's response now reflects the occurrence of an event, which in this case was the input current step.

#### C. Sinusoidal Response

We use sinusoidal currents to demonstrate  $I_T$ 's graded behavior. We begin with a  $4\text{Hz}$  input current, selecting the response mode by using two different mean current levels. In tonic-mode, the cell spikes during the sinusoid's upward half (Fig. 6a). In burst-mode, the cell bursts during the sinusoid's rising phase (Fig. 6b). These responses are similar to those elicited by the step.

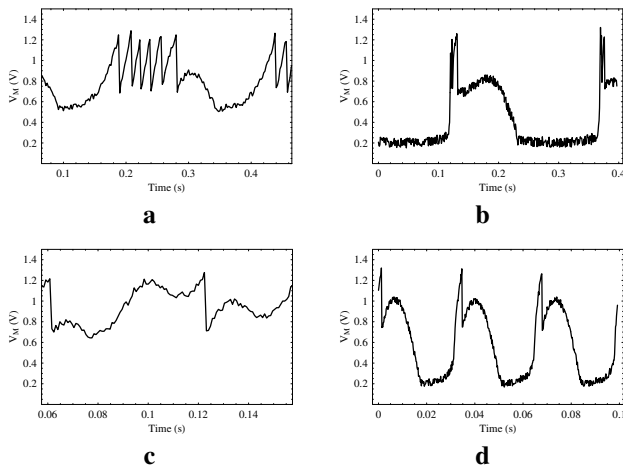


Fig. 6. Dendritic voltage ( $V_M$ ) records of the relay cell's response in tonic-mode (a, c) and burst-mode (b, d) to 4Hz (a, b) and 30Hz (c, d) sinusoidal input currents. The burst and tonic responses for each frequency have been aligned by phase.

At 30Hz, the cell responds subharmonically in tonic-mode but still phase-locks in burst-mode. With the high-mean input, which inactivates  $I_T$ , the cell integrates over multiple cycles and fires at a random phase (Fig. 6c). With the low-mean input, which deinactivates  $I_T$ , the cell manages to respond during each cycle (Fig. 6d); however, it fires only one spike (instead of a burst) since  $V_M$  spends less time low, preventing the T-channel from deinactivating fully.

For a series of frequencies, we observe no filtering in tonic-mode and bandpass filtering in burst-mode (Fig. 7a). In tonic-mode (blue), the cell maintains a (relatively) constant level of output activity, from multiple spikes per cycle at low frequencies to subharmonic spikes at high frequencies. In burst-mode (black), the number of spikes per cycle remains relatively constant at low frequencies, since the channel deinactivates fully each cycle, and so the average firing rate increases as the period shortens. As the frequency increases, the duration that  $V_M$  is low becomes shorter, and eventually the T-channel no longer deinactivates fully. This causes the number of spikes to decrease per cycle, as we demonstrated in Fig. 6d. Eventually, the T-channel cannot deinactivate, and the cell stops firing.

We observe a gradual transition from bandpass to allpass as we increase the mean current level. Two intermediate states are shown in Fig. 7a (red and green); they show characteristics of both firing modes. As the mean input current increases,  $V_M$  does not drop as much during the sinusoid's troughs, and so  $I_T$  does not deinactivate as much (see Fig. 3b for its voltage-dependence). The diminished burst response is evident in the bandpass' reduced peak. Conversely, the higher mean produces larger tonic responses at low frequencies due to the larger currents at the sinusoid's peaks.

With respect to phase, burst-mode leads while tonic-mode lags (Fig. 7b). The burst-mode's lead arises because the T-channel induces a burst before the sinusoid peaks. At high frequencies, the burst lags because there is a fixed delay between triggering and spiking. The tonic-mode always lags, since it relies on integration of the input. At low frequencies, this integration lag is negligible; as the period shortens, the latency becomes significant, causing a greater phase lag.

The two intermediate states follow the phase of the dominant mode (burst or tonic). At the low frequencies, where tonic dominates, the phase of both intermediate states approach the tonic phase curve. As the input frequency increases, burst starts to dominate, and their

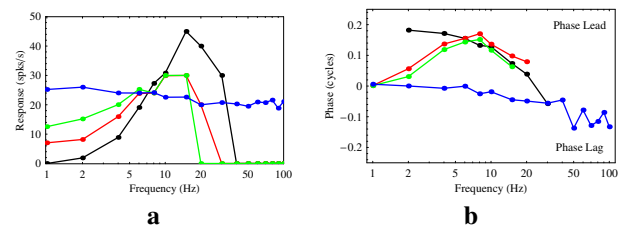


Fig. 7. Relay cell's frequency response for different firing modes: burst (black), tonic (blue) and burst-tonic (red and green). The response amplitude (a) and phase (b) are extracted from the Fourier transform of the output peristimulus time histogram (PSTH), each trial corresponding to a single cycle [6].

phases diverge from the tonic curve, approaching the burst curve.

#### IV. CONCLUSION

In this paper, we presented a silicon model of the thalamic relay cell. For the T-channel circuit, we used a previously published ion channel design for activation [2], but created a new circuit for inactivation that realizes its longer time-constants. We attached the T-channel circuit to a two-compartment silicon neuron. Using current inputs, we demonstrated the cell's different firing modes, and also the burst-mode's graded behavior.

For the cell to burst, its dendritic voltage must remain low for some duration to prime the T-channel. In the brain, surrounding the thalamus is a thin layer of inhibitory cells; they can drive the relay cells' voltages low and deinactivate the T current [7]. Corticothalamic feedback axons also excite these inhibitory cells, providing a means for cortex to control the thalamus' firing mode.

With a population of these silicon relay cells on our chip, we intend to study the influence of attention (i.e., cortical feedback) on sensory information passing through the thalamus. Evidence points to the involvement of both the thalamus [1] and the reticular nucleus [8] in attention. In particular, we plan to explore Francis Crick's "searchlight" hypothesis, which postulates that bursts are the expression of attention [9].

#### REFERENCES

- [1] M. Beierlein, C. P. Fall, J. Rinzel, and R. Yuste, "Thalamocortical bursts trigger recurrent activity in neocortical networks: layer 4 as a frequency-dependent gate," *J Neurosci*, vol. 22, no. 22, pp. 9885–94, 2002.
- [2] K. Hynna and K. Boahen, "Neuronal ion-channel dynamics in silicon," in *Circuits and Systems, 2006. ISCAS 2006. Proceedings. 2006 IEEE International Symposium on*, 2006, p. 4 pp.
- [3] K. Hynna, "T channel dynamics in a silicon LGN," Ph.D. dissertation, University of Pennsylvania, 2005.
- [4] K. A. Zaghoul and K. Boahen, "Optic nerve signals in a neuromorphic chip ii: Testing and results," *IEEE Transactions on Biomedical Engineering*, vol. 51, no. 4, pp. 667–675, 2004.
- [5] D. A. McCormick and H. R. Feeseer, "Functional implications of burst firing and single spike activity in lateral geniculate relay neurons," *Neuroscience*, vol. 39, no. 1, pp. 103–13, 1990.
- [6] G. D. Smith, C. L. Cox, S. M. Sherman, and J. Rinzel, "Fourier analysis of sinusoidally driven thalamocortical relay neurons and a minimal integrate-and-fire-or-burst model," *J Neurophysiol*, vol. 83, no. 1, pp. 588–610, 2000.
- [7] D. Ulrich and J. R. Huguenard, "GABA(A)-receptor-mediated rebound burst firing and burst shunting in thalamus," *J Neurophysiol*, vol. 78, no. 3, pp. 1748–51, 1997.
- [8] K. McAlonan and V. J. Brown, "The thalamic reticular nucleus: more than a sensory nucleus?" *Neuroscientist*, vol. 8, no. 4, pp. 302–5, 2002.
- [9] F. Crick, "Function of the thalamic reticular complex: the searchlight hypothesis," *Proc Natl Acad Sci U S A*, vol. 81, no. 14, pp. 4586–90, 1984.